DOI: 10.1002/chem.200701532

Torsional Angular Dependence of ^{1}J(Se,Se) and Fermi Contact Control of ^{4}J(Se,Se): Analysis of ^{n}J(Se,Se) ($n=1$–4) Based on Molecular Orbital Theory

Waro Nakanishi* and Satoko Hayashi[a]

Abstract: ^{n}J(Se,Se) ($n=1$–4) nuclear couplings between Se atoms were analyzed by using molecular orbital (MO) theory as the first step to investigating the nature of bonded and nonbonded ^{n}J(Se,Se) interactions between Se atoms. The values were calculated by employing Slater-type triple ξ basis sets at the DFT level, which were applied to structures optimized with the Gaussian 03 program. The contribution from each occupied MO (ψ_i) and $\psi_i \rightarrow \psi_a$ (ψ_a = unoccupied MO) transition was evaluated separately. ^{1}J(Se,Se) was calculated for the MeSeSeMe model compound, which showed a typical dependence on the torsion angle ($\phi(C_{Me}SeSeC_{Me})$). This dependence explains the small values (≤ 64 Hz) of $^{1}J_{obsd}$(Se,Se) observed for RSeSeR′ and large values (330–380 Hz) of $^{1}J_{obsd}$(Se,Se) observed for 4-substituted naphtho[1,8-*c*,*d*]-1,2-diselenoles, which correspond to synperiplanar diselenides. The HOMO→LUMO and HOMO−1→LUMO transitions contribute the most to ^{1}J(Se,Se) at $\phi=0$ and 180° to give large values of ^{1}J(Se,Se), whereas various transitions contribute and cancel each other out at $\phi=90°$ to give small values of ^{1}J(Se,Se). Large $^{4}J_{obsd}$(Se,Se) values were also observed in the nonbonded Se···Se, Se···Se=O, and O=Se···Se=O interactions at naphthalene 1,8-positions. The Fermi contact (FC) term contributes significantly to ^{4}J(Se,Se), whereas the paramagnetic spin-orbit (PSO) term contributes significantly to ^{1}J(Se,Se). ^{2}J(Se,Se) and ^{3}J(Se,Se) were analyzed in a similar manner and a torsional angular dependence was confirmed for ^{3}J(Se,Se). Depending on the structure, the main contribution to ^{n}J(Se,Se) ($n=2$, 3) is from the FC term, with a lesser contribution from the PSO term. Analysis of each transition enabled us to identify and clearly visualize the origin and mechanism of the couplings.

Keywords: ab initio calculations · coupling constants · NMR spectroscopy · selenium

Introduction

NMR spectroscopy has been established as an extremely powerful tool to study physical, chemical, and biological sciences. ^{77}Se NMR chemical shifts are used on a daily basis to determine molecular structures. Indirect nuclear spin–spin coupling constants (J) provide important information on coupled nuclei that contain strongly bonded or weakly interacting states because the values depend on the electron distribution between the nuclei.[1–6] One-bond (^{1}J), two-bond (*geminal*; ^{2}J), three-bond (*vicinal*; ^{3}J), and even longer (^{n}J; $n\geq 4$) coupling constants are observed between selenium atoms, which give important information about the coupled nuclei. For ^{1}J, the coupling mechanism is through-bond only, whereas the coupling mechanism for ^{n}J ($n\geq 2$), and in particular ^{n}J ($n\geq 4$), must contain through-space interactions. Quantum chemical (QC) calculations are necessary for the analysis and interpretation of the J values obtained experimentally. Important molecular properties, such as electronic structure, can be clarified by elucidating the mechanism of spin–spin couplings with molecular orbital (MO) theory. Scheme 1 shows the structures of the compounds used in this study.

Various values of $^{1}J_{obsd}$(Se,Se) have been reported for the alkyl and aryl derivatives of **1a** (Scheme 1). These values are usually small, for example, $^{1}J_{obsd}$(Se,Se) for **1** is ≤ 64 Hz (Table 1). However, we encountered large values of $^{1}J_{obsd}$(Se,Se) = 330 to 380 Hz for the derivatives of **2** (see Scheme 1 and Table 1), which correspond to the synperiplanar diselenides.[7,8] Values of $^{2}J_{obsd}$(Se,Se) are not reported

[a] Prof. Dr. W. Nakanishi, Dr. S. Hayashi
Department of Material Science and Chemistry
Faculty of Systems Engineering
Wakayama University
930 Sakaedani
Wakayama 640-8510 (Japan)
Fax: (+81) 73-457-8253
E-mail: nakanisi@sys.wakayama-u.ac.jp

Supporting information for this article is available on the WWW under http://www.chemeurj.org/ or from the author.

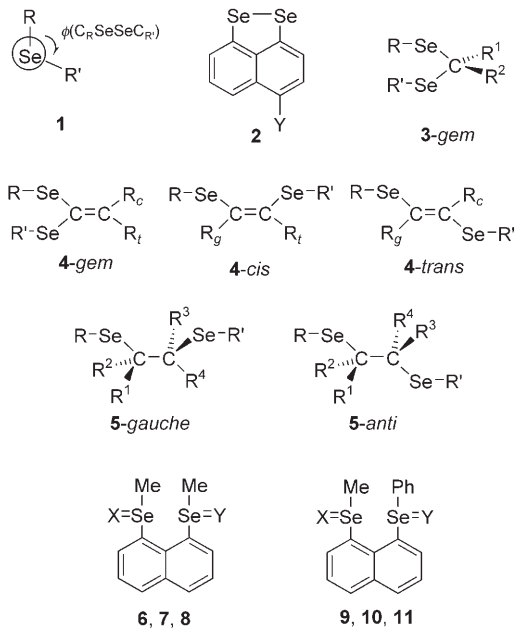

Scheme 1. Structures of the compounds used in this study. Specific substituents: **1a**: R = R′ = Me; **2a**:[7] Y = H; **2b**: Y = Me; **2c**: Y = Cl; **2d**: Y = NO_2; **3a**: R = R′ = Me, $R^1 = R^2 = H$; **4a**-*gem*: R = Me, R′ = R_c = Ph, R_t = H; **4a**-*cis*: R = R′ = Me, R_g = Ph, R_t = H; **4a**-*trans*: R = R′ = Me, R_g = Ph, R_c = H; **4b**: R = R′ = Me, $R_c = R_t = R_g$ = H; **5a**: R = R′ = Me, $R^1 = R^2 = R^3 = R^4$ = H; **6** and **9**: X = Y = null; **7** and **10**: X = O, Y = null; **8** and **11**: X = Y = O.

for **3**-*gem*,[9] but values for **4a**-*gem*[4,10a] are given in Table 1, together with values of $^3J_{obsd}$(Se,Se) for **4a**-*cis* and **4a**-*trans*.[4,10] Values for **5**-*gauche* and **5**-*anti* must also be considered. The values of ^4J(Se,Se), such as in **6**, **7**, and **8**, are closely related to nonbonded Se···Se interactions. Large values of $^4J_{obsd}$(Se,Se) were detected for **7**, **9**,[11] **10**, and **11**.

According to nonrelativistic theory, there are several mechanisms that contribute to the spin–spin coupling constants.[12] As expressed in Equation (1), the total value ($^nJ_{TL}$) is composed of contributions from the diamagnetic spin-orbit (DSO) term, the paramagnetic spin-orbit (PSO) term, the spin-dipolar (SD) term, and the Fermi contact (FC) term.

$$^nJ_{TL} = {}^nJ_{DSO} + {}^nJ_{PSO} + {}^nJ_{SD} + {}^nJ_{FC} \quad (1)$$

Figure 1 summarizes the mechanism of the indirect nuclear spin–spin couplings and illustrates the origin of the $^nJ_{DSO}$, $^nJ_{PSO}$, $^nJ_{SD}$, and $^nJ_{FC}$ terms and their contribution to $^nJ_{TL}$. The singlet state (S_0) of a molecule (**M**) is the ground state if the nuclei (N) in **M** have no magnetic moments ($\mu_N = 0$), but the ground state cannot be the absolute S_0 if $\mu_N \neq 0$. The contributions to the μ_N-perturbed ground state are as follows: The DSO term arises from the reorganization of S_0, so it is usually very small. The PSO term arises from the mixing of upper singlet states (S_1, S_2, S_3, etc.) and the FC and SD terms arise from admixtures of upper triplet states (T_1, T_2, T_3, etc.), in which only s-type atomic orbitals contribute to FC.

Why is the value of $^1J_{obsd}$(Se,Se) for **2** much larger than that of **1**? Why are the values of $^4J_{obsd}$(Se,Se) in **7** and **9**–**11** so large despite nonbonded Se···Se distances of about 3 Å?[11] The values of ^nJ(Se,Se) (n = 1–4) were analyzed by using MO theory to investigate the nature of the bonded and nonbonded interactions between selenium atoms through nuclear spin–spin coupling. How do Se nuclei interact with each other to contribute to ^nJ(Se,Se)? Mechanisms for Se···Se interactions at bonded and nonbonded distances have been elucidated. Calculated $^nJ_{TL}$ values were evaluated separately by using the four terms shown in Equation (1). A precise description of the electron density at the coupled nuclei is required to evaluate the FC contribution, however, satisfactory accuracy would be difficult to achieve by using Gauss-type atomic orbitals. Therefore, J values were evaluated by using Slater-type atomic orbitals, which is possible when using the ADF 2005 program.[13,14] Evaluation of the J values was performed by using the ADF program after structural optimization with the Gaussian 03 program.[15] Contributions from each occupied MO (ψ_i) and $\psi_i \rightarrow \psi_a$ (ψ_a = unoccupied MO) transition were evaluated separately. The treatment enabled us to identify and clearly visualize the origin of the indirect nuclear spin–spin couplings.

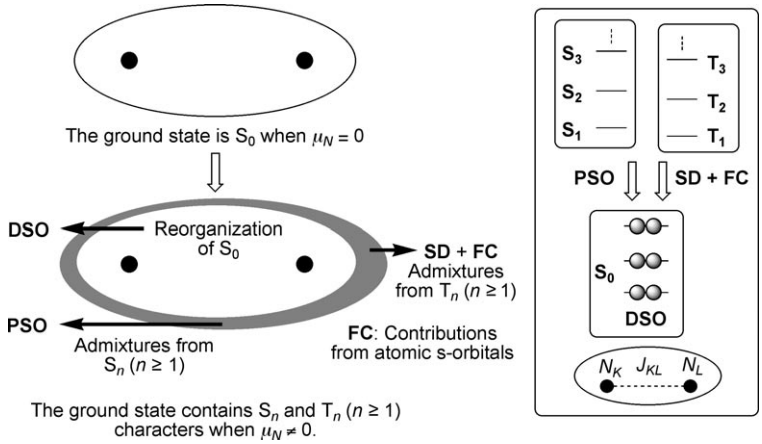

Figure 1. The mechanisms of indirect nuclear spin–spin couplings and the origin of the $^nJ_{DSO}$, $^nJ_{PSO}$, $^nJ_{SD}$, and $^nJ_{FC}$ terms that contribute to $^nJ_{TL}$. S = singlet state, T = triplet state, N = nuclei, and μ = magnetic moment.

Results and Discussion

Observed $^nJ_{obsd}$(Se,Se) (n = 1–4) values: The magnitude of the values of $^1J_{obsd}$(Se,Se) are usually small, and values of < 64 Hz were observed for compounds **1**.[4,16] However, large values of $^1J_{obsd}$(Se,Se) were recorded for **2b**–**d** (see Table 1), which are synperiplanar diselenides, although not for **2a**.[7] It was expected that the values of ^1J(Se,Se) would

Table 1. Observed spin–spin coupling constants ($^nJ_{obsd}$) between Se atoms.

	n	$^nJ_{obsd}$(Se,Se) [Hz]	Interaction
1 (R = *t*Bu, R′ = Me)[a]	1	2.7	Se–Se
1 (R = *n*Bu, R′ = Me)[a]	1	36.3	Se–Se
1 (R = Me, R′ = Ph)[a]	1	22	Se–Se
1 (R = *o*$O_2NC_6H_4$, R′ = CN)[b]	1	64	Se–Se
2b[c]	1	379.4	Se–Se
2c[c]	1	375.9	Se–Se
2d[c]	1	330.8	Se–Se
4a-*gem*[d]	2	27	Se···Se
4a-*cis*[d]	3	96.5	Se···Se
4a-*trans*[d]	3	12.0	Se···Se
9[c]	4	332.4	Se···Se
7[c]	4	199.5	O=Se···Se
10[c]	4	188.5	O=Se···Se
11[c]	4	455.8	O=Se···Se=O

[a] Refs. [4] and [16a]. [b] Refs. [4] and [16b]. [c] This work. [d] Refs. [4] and [10a].

be controlled by the torsion angle (ϕ(CSeSeC)) because this effect is well-known in three-bond (*vicinal*) couplings in ^{1}H NMR spectra.[1] Values of $^2J_{obsd}$(Se,Se) and $^3J_{obsd}$(Se,Se) have been reported for **4a**-*gem*, **4a**-*cis*, and **4a**-*trans*;[4,10] the magnitudes of which are not very large (Table 1).

A value of $^4J_{obsd}$(Se,Se) = 199.5 Hz was recorded for **7** and values of $^4J_{obsd}$(Se,Se) = 332.4, 188.5, and 455.8 Hz were observed for methyl phenyl derivatives **9**, **10**, and **11**, respectively. To the best of our knowledge, the $^4J_{obsd}$(Se,Se) value of 455.8 Hz obtained for **11** is largest value observed to date. The values of $^4J_{obsd}$(Se,Se) observed for **7** and **10** were very close (Table 1), which suggests that substituting a methyl group with a phenyl group at the naphthalene 1,8-positions does not affect $^4J_{obsd}$(Se,Se) much.

After briefly summarizing the $^nJ_{obsd}$(Se,Se) (n = 1–4) values obtained, the next step is to elucidate the ^nJ(Se,Se) coupling mechanisms by using MO theory to investigate the nature of chemically bonded and weakly interacting selenium atoms.

Calculation method: The structures of **1a** and **3–5** were optimized by using the 6-311++G(3df,2pd) basis sets of the Gaussian 03 program[15,17] at the DFT (B3LYP) level.[18–20] In the fully optimized structure of **1a**, ϕ(C_{Me}SeSeC_{Me}) was calculated to be 88.38°. Calculations were also performed on structures of **1a** with fixed torsion angles altered in increments of 15 or 30° (see Table 2). Structural optimization was also performed on **3a** and some conformers of **4b**[21] and **5a**. Optimizations were also performed on **2a**, **6–8**, 1,8-$(HSe)_2C_{10}H_6$ (**12**), and 1,8-$(HSe=O)_2C_{10}H_6$ (**13**) by using the 6-311+G(3df) basis sets[17] for Se and the 6-311+G(3d,2p) basis sets for other nuclei at the DFT (B3LYP) level.[18] The values of J(Se,Se) were calculated by using Slater-type triple ξ basis sets with two sets of polarization functions (2×1s, 2×2s, 2×2p, 2×3s, 2×3p, 3×3d, 3×4s, 3×4p, 1×4d, and 1×4f for Se) at the DFT (BLYP) level of the ADF 2005 program[13] on the optimized structures obtained with the Gaussian 03 program.[15,20] Calculations were performed at the nonrelativistic level. For ease of comparison, the scalar ZORA relativistic formulation[22] was also applied to **2a** and **12** (**BB**).[23] The $^nJ_{TL}$ values were evaluated separately by using the $^nJ_{DSO}$, $^nJ_{PSO}$, $^nJ_{SD}$, and $^nJ_{FC}$ terms in Equation (1)].[12] The mechanism was revealed by determining the contribution from each ψ_i and $\psi_i \rightarrow \psi_a$ transition.[24]

Analysis of ^1J(Se,Se): Table 2 shows $^1J_{TL}$ and the $^1J_{DSO}$, $^1J_{PSO}$, $^1J_{SD}$, and $^1J_{FC}$ components calculated for ^1J(Se,Se) in **1a**. The predicted value of $^1J_{TL}$(Se,Se) in **1a** is very large at ϕ = 0° (684 Hz) and 180° (628 Hz), whereas it is less than 44 Hz for ϕ = (90±15)°. Therefore, the $^1J_{obsd}$(Se,Se) value obtained for **1** can be substantially explained and modeled by using **1a** at $\phi \approx 90°$, although changes to R and R′ in **1** must also affect the values. Figure 2 shows plots of $^1J_{DSO}$, $^1J_{PSO}$, $^1J_{SD}$, $^1J_{FC}$, $^1J_{SD+FC}$, and $^1J_{TL}$ versus ϕ in **1a**. The results show that $^1J_{TL}$ is

Table 2. Calculated values of ^1J(Se,Se) for **1a** and **2a**, together with the torsional angular dependence in **1a**.[a]

	ϕ [°]	E_{rel}[b] [kJ mol^{-1}]	$^1J_{PSO}$ [Hz]	$^1J_{SD}$ [Hz]	$^1J_{FC}$ [Hz]	$^1J_{SD+FC}$ [Hz]	$^1J_{TL}$ [Hz]
1a	0.0	36.9	447.2	217.8	18.6	236.4	683.7
	15.0	33.0	399.2	200.6	15.2	215.8	615.0
	30.0	25.3	288.5	163.1	2.7	165.8	454.3
	60.0	6.1	76.1	101.4	−43.3	58.1	134.2
	75.0	0.9	20.0	87.8	−64.7	23.1	43.1
	88.4	0.0	4.1	84.5	−76.7	7.8	11.9
	90.0	0.0	4.2	84.6	−77.9	6.7	10.9
	105.0	2.3	29.9	91.5	−77.4	14.1	44.0
	120.0	7.4	94.7	109.3	−60.5	48.8	143.5
	150.0	17.6	291.5	171.7	−8.2	163.5	455.0
	165.0	21.5	370.6	201.1	9.0	210.1	580.7
	180.0	22.8	400.7	213.4	14.3	227.7	628.4
2a	–	–	362.2	195.2	−54.1	141.1	503.3
2a[c]	–	–	390.7	206.4	2.6	209.0	599.7

[a] $^1J_{DSO}$ was less than 0.03 Hz. [b] E_{rel} is the energy value relative to the optimized value of −5267.7384 a.u. obtained at ϕ = 88.38°. [c] Based on scalar ZORA.

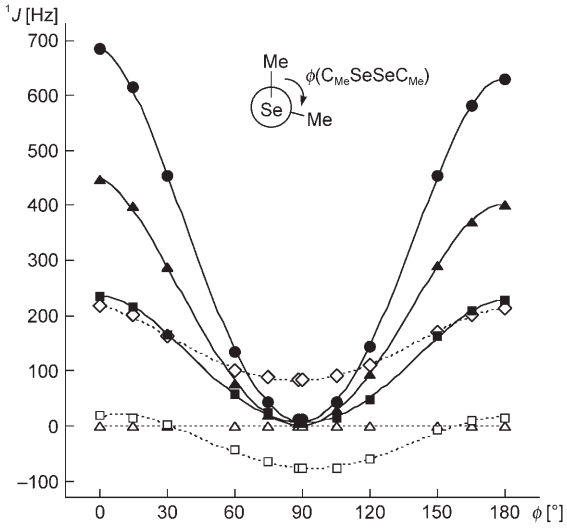

Figure 2. Torsional angular dependence of ^1J(Se,Se) in **1a**. △: $^1J_{DSO}$, ▲: $^1J_{PSO}$, ◇: $^1J_{SD}$, □: $^1J_{FC}$, ■: $^1J_{SD+FC}$, and ●: $^1J_{TL}$.

dependent on ϕ, which is also true for ^3J(H,H);[1] and changes to $^1J_{DSO}$ were also negligible (<0.03 Hz).

$^1J_{PSO}$(Se,Se) and $^1J_{SD+FC}$(Se,Se) were plotted against $^1J_{TL}$(Se,Se) for **1a**.[12] The correlations are given in Equations (2) and (3), respectively. The results showed that for **1a** $^1J_{PSO}$(Se,Se) and $^1J_{SD+FC}$(Se,Se) contribute 65 and 35%, respectively, to $^1J_{TL}$(Se,Se), irrespective of the values of ϕ(CSeSeC).

$$^1J_{PSO}(\mathrm{Se,Se}) = 0.651 \times {}^1J_{TL}(\mathrm{Se,Se}) - 4.1 \quad (r^2 = 0.999) \qquad (2)$$

$$^1J_{SD+FC}(\mathrm{Se,Se}) = 0.349 \times {}^1J_{TL}(\mathrm{Se,Se}) + 4.2 \quad (r^2 = 0.998) \qquad (3)$$

The value of ^1J(Se,Se) for **1a** was predicted to be very large when $\phi = 0$ or 180°. Consequently, for **2** a value of $^1J_{obsd}(\mathrm{Se,Se}) = 331$ to 379 Hz could be predicted from the ^1J(Se,Se) value for **1a** when $\phi = 0°$ (Table 2). A value of $^1J_{TL}(\mathrm{Se,Se}) = 503$ Hz was calculated for **2a**, of which the $^1J_{PSO}$(Se,Se) value for **2a** contributes 72% (Table 2). The predicted value of $^1J_{TL}$(Se,Se) for **2a** is about 120 Hz larger than the $^1J_{obsd}$(Se,Se) value obtained for **2b**. The DFT method overestimates the reciprocal energy differences $(1/(\varepsilon_a - \varepsilon_i))$[12] that would be partly responsible for the larger value.

Why does the value of ^1J(Se,Se) for **1a** depend on the torsion angle? Which orbitals and transitions contribute to this dependence? To answer these questions, we examined $^1J_{PSO}$(Se,Se) for **1a** because it contributes 65% to $^1J_{TL}$(Se,Se). The mechanism discussed herein is based on the contributions from each ψ_i and $\psi_i \rightarrow \psi_a$ transition. Table 3 lists the dependence of $^1J_{PSO}$(Se,Se) on ϕ for **1a** and contributions from ψ_1–ψ_{43}, ψ_1–ψ_{38}, ψ_{39}–ψ_{43}, ψ_{39}, ψ_{40}, ψ_{41}, ψ_{42}, and ψ_{43}. The contribution of ψ_{39}–ψ_{43} to the $^1J_{PSO}$(Se,Se) value of **1a** is large, whereas that of ψ_1–ψ_{38} is small.[25] Figure 3a shows the contributions from ψ_{39}, ψ_{40}, ψ_{41}, ψ_{42}, and ψ_{43} and Figure 3b shows the contributions from ψ_{39}–ψ_{41}, ψ_{42}–ψ_{43}, and ψ_{39}–ψ_{43}. The contributions from ψ_{42} and ψ_{43} exchange with each other at $\phi \approx 90°$ and the contributions from ψ_{39} and ψ_{40} exchange at $\phi \approx 135°$ (Figure 3a). The contributions from ψ_{42}–ψ_{43} and ψ_{39}–ψ_{41} almost cancel each other out at $\phi \approx 90°$ (Figure 3b).

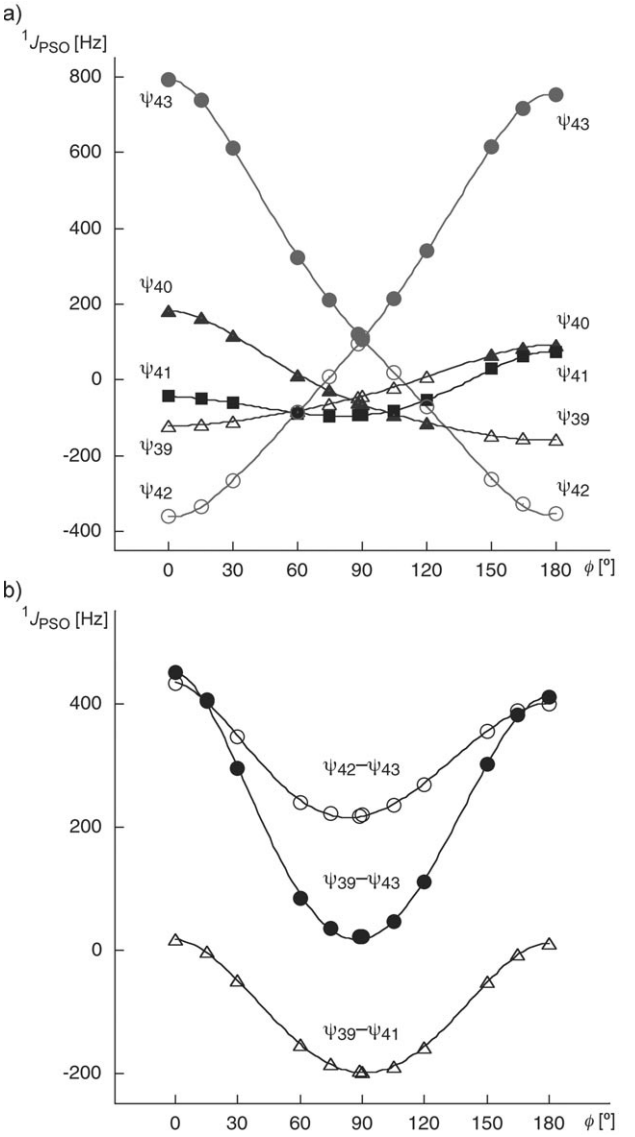

Figure 3. Torsional angular dependence of $^1J_{PSO}$(Se,Se) in **1a**. a) Contributions from ψ_{39}, ψ_{40}, ψ_{41}, ψ_{42}, and ψ_{43} and b) contributions from ψ_{39}–ψ_{41}, ψ_{42}–ψ_{43}, and ψ_{39}–ψ_{43}.

Table 3. Torsional angular dependence of the contributions to $^1J_{PSO}$(Se,Se) in **1a** from ψ_i.[a]

ϕ [°]	Contributions [Hz]									
	ψ_1–ψ_{43}	ψ_1–ψ_{38}	ψ_{39}–ψ_{43}	ψ_{39}	ψ_{40}	ψ_{41}	ψ_{42}	ψ_{43}	$\psi_{42}\rightarrow\psi_{44}$[b]	$\psi_{43}\rightarrow\psi_{44}$[b]
0.0	447.2	−2.7	449.9	−121.2	181.2	−43.3	−359.7	792.9	−333.3	747.2
15.0	399.2	−3.9	403.1	−117.6	163.4	−48.3	−333.7	739.4	−307.1	695.7
30.0	288.5	−6.4	294.9	−108.9	118.7	−60.8	−266.1	612.0	−240.9	574.7
60.0	76.1	−8.4	84.4	−80.9	13.7	−87.9	−84.0	323.7	−69.4	312.4
75.0	19.9	−15.2	35.2	−63.0	−28.6	−94.3	9.6	211.5	15.6	206.8
88.4	4.1	−16.3	20.4	−44.9	−59.4	−93.1	95.6	122.2	93.3	125.9
90.0	4.3	−16.3	20.6	−42.6	−62.8	−92.4	111.9	106.5	116.5	103.2
105.0	29.9	−16.0	45.9	−18.9	−90.8	−79.9	21.2	214.3	33.2	202.0
120.0	94.7	−14.4	109.1	8.7	−114.3	−54.0	−71.9	340.7	−54.4	320.7
150.0	291.4	−10.8	302.2	−146.9	65.3	28.7	−261.5	616.6	−235.6	581.5
165.0	370.5	−9.8	380.3	−155.1	85.4	62.4	−328.1	715.7	−298.1	673.8
180.0	400.7	−9.7	410.4	−157.7	93.0	75.0	−352.7	752.8	−321.0	708.6

[a] $^1J_{DSO}$ was less than 0.03 Hz. [b] Contribution from the transition.

The magnitudes of the contributions from ψ_{42} and ψ_{43} to the $^1J_{PSO}$(Se,Se) value of **1a** are very large at 0 and 180° (Table 3), although the signs of ψ_{42} and ψ_{43} are negative and positive, respectively. The values are −360 and −353 Hz for ψ_{42}, and 793 and 753 Hz for ψ_{43} at 0 and 180°, respectively.

The contributions from ψ_{42}–ψ_{43} are 433, 218, and 400 Hz at 0, 90, and 180°, respectively, and those from ψ_{39}–ψ_{41} are 17, −198, and 10 Hz at 0, 90, and 180°, respectively. Therefore,

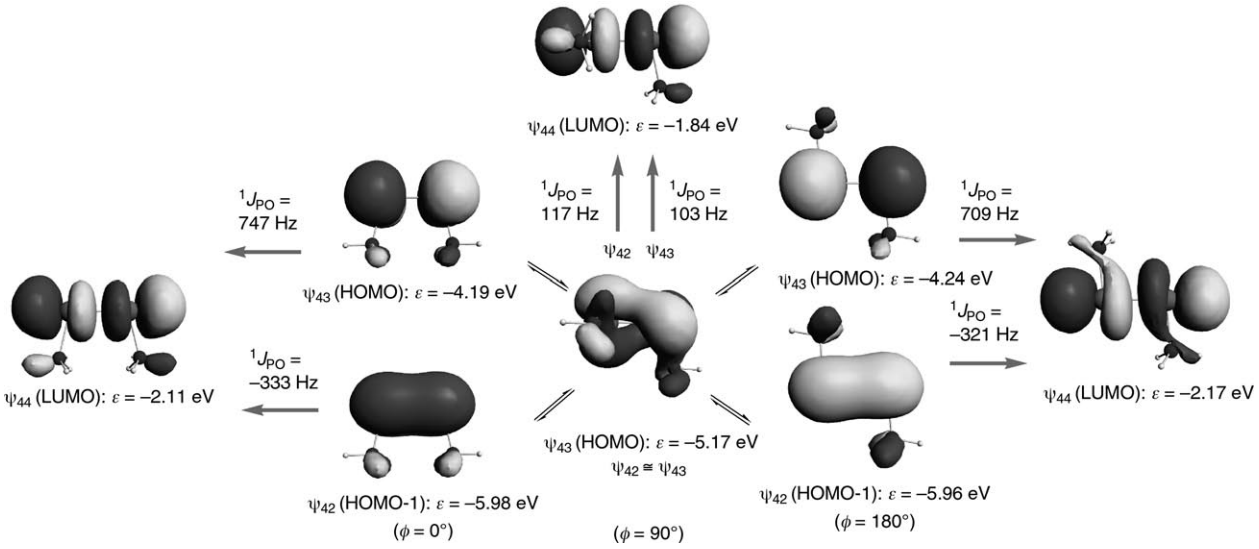

Figure 4. Contributions to $^1J_{PSO}$(Se,Se) in **1a** from the $\psi_{42}\rightarrow\psi_{44}$ and $\psi_{43}\rightarrow\psi_{44}$ transitions at $\phi=0$, 90, and 180°, together with the interconversion between ψ_{42} and ψ_{43} at $\phi\approx90°$.

the mechanism of $^1J_{PSO}$(Se,Se) in **1a** can be clarified by analyzing the contributions from ψ_{42} and ψ_{43} at 0 and 180°. The mechanism would be complex at 90°, since the small magnitude is a result of the total contributions from ψ_{39}–ψ_{43}.

Figure 4 shows the $\psi_{42}\rightarrow\psi_{44}$ and $\psi_{43}\rightarrow\psi_{44}$ transitions at $\phi=0$ and 180°, the values of which are shown in Table 3. The characters at $\phi=0$ and 180° of ψ_{42}(HOMO−1), ψ_{43}(HOMO), and ψ_{44}(LUMO) are π(Se–Se), π*(Se–Se), and σ*(Se–Se), respectively. The character of ψ_{42} is essentially the same as ψ_{43} at $\phi=90°$. To demonstrate how they interconvert with each other at $\phi=90°$, ψ_{42} and ψ_{43} are also shown in Figure 4. At $\phi\approx90°$ all of ψ_{39}–ψ_{43} contribute to $^1J_{PSO}$(Se,Se) in **1a**, contrary to the situation at $\phi\approx0$ or 180°. At 90°, contributions from the $\psi_{42}\rightarrow\psi_{44}$ and $\psi_{43}\rightarrow\psi_{44}$ transitions to $^1J_{PSO}$(Se,Se) in **1a** are almost cancelled by those from the $\psi_{39}\rightarrow\psi_{44}$, $\psi_{40}\rightarrow\psi_{44}$, and $\psi_{41}\rightarrow\psi_{44}$ transitions. In addition, both $^1J_{SD}$(Se,Se) and $^1J_{FC}$(Se,Se) in **1a** substantially contribute at $\phi\approx90°$. Consequently, it is difficult to specify a few orbitals and transitions that control ^1J(Se,Se) in **1a** at $\phi\approx90°$. The character of ψ_{44}(LUMO: σ*(Se–Se)) does not depend as much on ϕ, so therefore, the behavior of ψ_{39}–ψ_{43} must be mainly responsible for the dependence of ^1J(Se,Se) on ϕ for **1a** (see Figure 3 and Figure 4). The MO description in Figure 4 visualizes the origin of $^1J_{PSO}$(Se,Se) in **1a** and helps us to understand the mechanism, especially at $\phi=0$ and 180°.

The origin of ^1J(Se,Se) in **2** was similarly elucidated by analyzing $^1J_{PSO}$(Se,Se) in **2a**, of which contributions from each ψ_i and $\psi_i\rightarrow\psi_a$ transition were evaluated separately. The calculated ^1J(Se,Se) value obtained for **2a** is also given in Table 2.[23] The contribution of $^1J_{PSO}$(Se,Se) to $^1J_{TL}$(Se,Se) amounts to 72% for **2a**. Figure 5 shows the contributions to

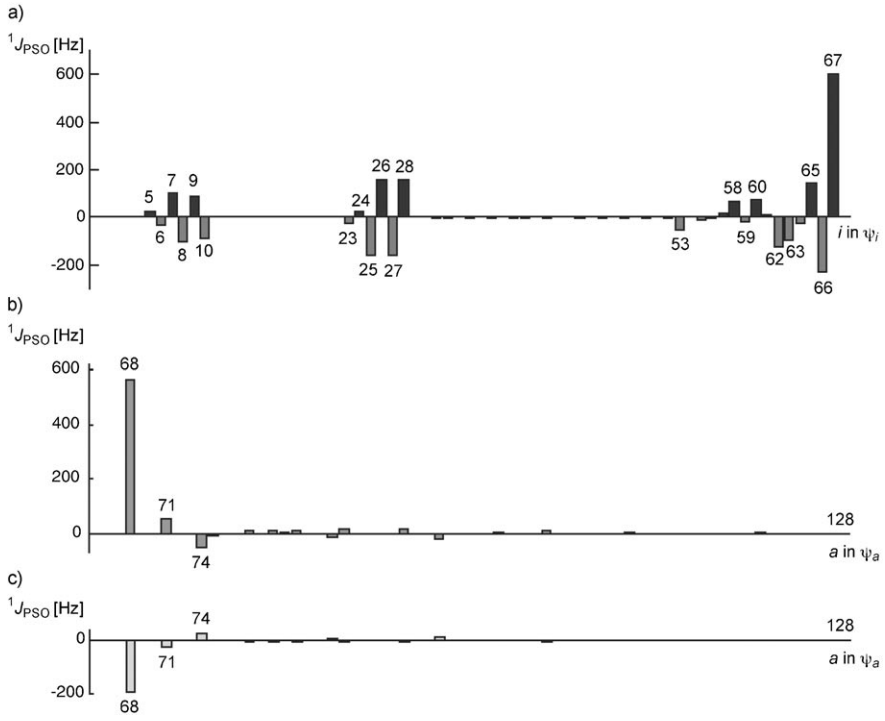

Figure 5. Contributions to $^1J_{PSO}$(Se,Se) in **2a** from a) each ψ_i, b) each $\psi_{67}\rightarrow\psi_a$ transition, and c) each $\psi_{66}\rightarrow\psi_a$ transition. ψ_{67} = HOMO, ψ_{66} = HOMO−1, and ψ_{68} = LUMO.

$^1J_{PSO}$(Se,Se) in **2a** from each ψ_i and the $\psi_{67}\rightarrow\psi_a$ and $\psi_{66}\rightarrow\psi_a$ transitions. In Figure 5a, contributions from ψ_5–ψ_{10}, ψ_{23}–ψ_{28}, and ψ_{53}–ψ_{67} originate mainly from atomic 2p(Se), 3p(Se), and 4p(Se) orbitals, respectively. The contributions that result from 2p(Se) and 3p(Se) are almost cancelled out by summing the contributions from ψ_5–ψ_{10} and ψ_{23}–ψ_{28}, respectively, therefore 4p(Se) substantially contributes to $^1J_{PSO}$(Se,Se) in **2a**. In particular, ψ_{67}(HOMO) and ψ_{66}(HOMO−1) control $^1J_{PSO}$(Se,Se) in **2a**. As shown in Figure 5b and c, the value of $^1J_{PSO}$(Se,Se) in **2a** is determined by $\psi_a=\psi_{68}$ when $\psi_i=\psi_{67}$ or ψ_{66} in many $\psi_i\rightarrow\psi_a$ transitions.[26]

Figure 6 shows the $\psi_{67}\rightarrow\psi_{68}$ and $\psi_{66}\rightarrow\psi_{68}$ transitions in $^1J_{PSO}$(Se,Se) for **2a**. The large value of $^1J_{PSO}$(Se,Se) for **2a** arises from mixing ψ_{68}(LUMO: σ*(Se–Se)) with ψ_{67}(HOMO: π*(Se–Se)) and ψ_{66}(HOMO−1: π(Se–Se)) in the singlet state. The MO shown in Figure 6 is essentially the same as the $\psi_{42}\rightarrow\psi_{44}$ and $\psi_{43}\rightarrow\psi_{44}$ transitions in $^1J_{PSO}$(Se,Se) for **1a** at $\phi=0°$ (Figure 4), although ψ_{67} (**2a**) and ψ_{66} (**2a**) also have π(Nap) (Nap = naphthyl) character. The large $^1J_{PSO}$(Se,Se) in **2** and small $^1J_{obsd}$(Se,Se) in **1** are explained by the dependence of the calculated ^1J(Se,Se) values in **1a** on ϕ.

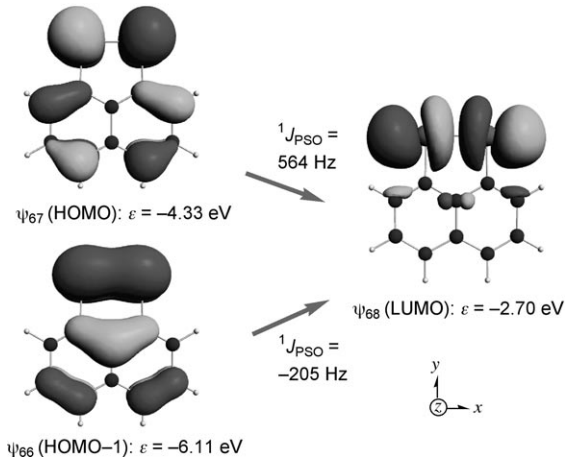

Figure 6. The $\psi_{67}\rightarrow\psi_{68}$ and $\psi_{66}\rightarrow\psi_{68}$ transitions in $^1J_{PSO}$(Se,Se) in **2a**. The characters of ψ_{67}, ψ_{66}, and ψ_{68} are π*(Se–Se), π(Se–Se), and σ*(Se–Se), respectively.

After elucidation of the mechanisms of ^1J(Se,Se), the next step is to clarify those for ^2J(Se,Se) in *geminal* bis-selenides, ^3J(Se,Se) in *vicinal* bis-selenides, and ^4J(Se,Se) in 1,8-bis(selanyl)naphthalenes.[27,28] Depending on the structure, ^2J(Se,Se) and ^3J(Se,Se) are mainly controlled by the FC term, with the PSO term being less important. However, the FC term definitely determines ^4J(Se,Se), so it is instructive to discuss the mechanisms of ^4J(Se,Se) before discussing those of ^2J(Se,Se) and ^3J(Se,Se).

Analysis of ^4J(Se,Se): Figure 7 shows the optimized structures for **6**, which are denoted by **6(AA)**, **6(AB)**, **6(BB)**, and **6(CC)**. Table 4 gives the energies of **6(AA)**, **6(AB)**, and **6(CC)** relative to **6(BB)**. Structure **6(CC)** is the global minimum and has been detected in crystal structures,[29] but **6(AB)** must be in equilibrium with **6(CC)** in solution. Structure **6(BB)** was shown to be the transition state with two negative (imaginary) frequencies.[30] Structures **7(AA)** and **8(AA)** were optimized as the global minima and correspond to the observed crystal structures. The other conformers optimized for **7** and **8** were higher energy species.

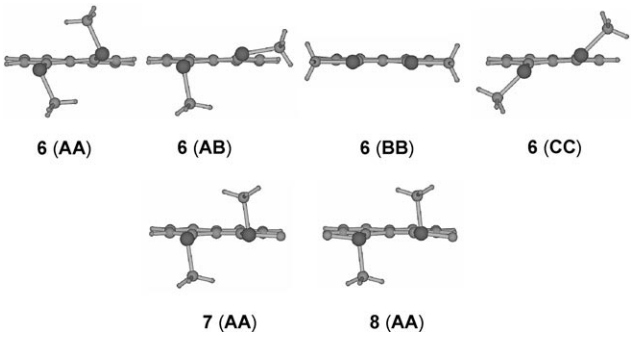

Figure 7. Optimized structures of **6**–**8**.

Table 4. Calculated values of ^4J(Se,Se) for **6**–**8**, **12**, and **13**.[a]

	E_{rel}[b] [kJ mol^{-1}]	$^4J_{PSO}$ [Hz]	$^4J_{SD}$ [Hz]	$^4J_{FC}$ [Hz]	$^4J_{TL}$ [Hz]
6(AA)	−5.3	10.2	−1.4	10.7	19.5
6(AB)	−20.7	1.1	−0.7	148.4	148.8
6(BB)	0.0	−0.5	−0.9	566.2	564.8
6(CC)	−23.4	2.6	0.2	399.2	402.0
7(AA)	–	0.8	−1.1	80.6	80.3
8(AA)	–	1.0	0.3	363.1	364.4
8(AA)*[c]	–	1.2	0.4	468.4	470.1
12(AB)	−5.0	3.9	0.0	127.8	131.8
12(BB)	0.0	0.7	−0.3	432.5	433.2
12(BB)[d]	0.0	−0.3	−0.8	415.1	414.0
12(CC)	−5.1	16.7	0.2	399.2	401.8
13(AA)	–	0.7	0.2	364.9	365.6

[a] $^1J_{DSO}$ was less than 0.06 Hz. [b] E_{rel} is the energy value relative to **6(BB)** (−5267.7358 a.u.), which contains the thermal effect at 273.15 K. [c] Calculated from the optimized structures with *r*(Se,Se) fixed at the observed value of 3.151 Å. [d] Based on scalar ZORA.

Table 4 shows values of ^4J(Se,Se) that were calculated for the optimized structures shown in Figure 7. $^4J_{FC}$(Se,Se) plays a definitive role (contribution of >99%, except in **6(AA)**) in determining $^4J_{TL}$(Se,Se) in **6**, **7** and **8**, which arises from nonbonded Se···Se, Se···Se=O, and O=Se···Se=O interactions, respectively. Values of $^4J_{TL}$(Se,Se) = 402 and 149 Hz were determined for **6(CC)** and **6(AB)**, respectively, and the observed value of 332 Hz for **9** is intermediate between the two. The results are consistent with an equilibrium between **6(CC)** and **6(AB)** in solution, even though a methyl group in **6** is replaced by a phenyl group in **9**. A very small value of $^4J_{TL}$(Se,Se) = 20 Hz was predicted for **6(AA)**, which is in striking contrast to the large $^1J_{TL}$(Se,Se) value of 503 Hz predicted for **2a**.

Values of $^4J_{TL}$(Se,Se) = 80 and 364 Hz were predicted for **7**(**AA**) and **8**(**AA**), respectively. These values are smaller than those observed for **7**, **10**, and **11** by about 90 to 120 Hz (Tables 1 and 4). Why do these differences arise? The nonbonded Se···Se distances were reexamined because they were optimized to be longer than the observed values by 0.095 and 0.134 Å for **7**(**AA**) and **8**(**AA**), respectively, and these longer distances could be responsible for the discrepancy. Structure **8**(**AA**) was optimized with *r*(Se,Se) fixed at the observed value of 3.151 Å and by assuming C_2 symmetry. Under these conditions, this optimized structure was designated **8**(**AA**)*, and has a ^4J(Se,Se) value of 470 Hz. This value is very close to that observed for **11**(**AA**) (456 Hz). From this, it can be seen that, in some cases, optimized *r*(Se,Se) distances must be carefully examined when discussing values of ^4J(Se,Se) based on the calculated values.

Values of $^4J_{FC}$(Se,Se) were examined by breaking down and examining the contributions from each ψ_i and $\psi_i \rightarrow \psi_a$ transition for **6**–**8** to clarify the mechanism for ^4J(Se,Se) that arises from nonbonded Se···Se, Se···Se=O, and O=Se···Se=O interactions. The MO presentations explain the mechanisms,[31] but they are too complex for the mechanisms to be easily understood because the MOs in **6**–**8** extend over whole molecules that contain two MeSe or MeSe=O groups and π(Nap) systems. To avoid this complexity, frontier molecular orbitals (FMOs) were drawn for **12** and **13**; the calculated values are shown in Table 4.[23]

The value of $^4J_{FC}$(Se,Se) = 433 Hz in **12**(**BB**) has a large (556 Hz) contribution from ψ_{64}. Contributions from the $\psi_{64} \rightarrow \psi_{70}$ (138 Hz), $\psi_{64} \rightarrow \psi_{72}$ (−485 Hz), and $\psi_{64} \rightarrow \psi_{74}$ (799 Hz) transitions amount to 452 Hz, which explains the value of $^4J_{FC}$(Se,Se) in **12**(**BB**). Namely, $^4J_{FC}$(Se,Se) originates mainly from admixtures of ψ_{70}, ψ_{72}, and ψ_{74} into ψ_{64}. Figure 8a shows the $\psi_{64} \rightarrow \psi_{72}$ and $\psi_{64} \rightarrow \psi_{74}$ transitions in **12**(**BB**). The character of ψ_{74} is a symmetrically combined double σ*(C_{Nap}–Se–H) of *a*-type (σ*(C_{Nap}–Se–H)-*a*), ψ_{72} is the antisymmetrically combined double σ*(C_{Nap}–Se), and ψ_{64} is the antisymmetrically combined double σ(C_{Nap}–Se–H)-*a*. Through interaction with π(Nap) ψ_{64} in **12**(**BB**) separates into ψ_{62} and ψ_{64} in **12**(**CC**). Figure 8b shows the FMOs of **12**(**CC**), which are exemplified by the $\psi_{62} \rightarrow \psi_{74}$ and $\psi_{64} \rightarrow \psi_{74}$ transitions. The FMOs of **6**(**BB**) and **6**(**CC**) are essentially the same as those of **12**(**BB**) and **12**(**CC**), respectively. The MOs of **6**(**BB**) and **6**(**CC**) were split further through interactions with the methyl groups, however, they are not shown here because of their high complexity.

Figure 9 shows the FMOs for **12**(**AB**), in which the main contribution is from the $\psi_{62} \rightarrow \psi_{74}$ transition. The transition in **12**(**AB**) seems to be more complex than that of **12**(**BB**) or **12**(**CC**). The smaller *J* value in **12**(**AB**) could come from the perpendicular conformations of two Se–H groups and two s-type lone-pair orbitals.[32]

Figure 10 shows the $\psi_{73} \rightarrow \psi_{80}$ transition in **13**(**AA**). This transition is reminiscent of the admixture of π orbitals along the linear O=Se···Se=O arrangement. However, the s-type atomic orbitals of Se found in ψ_{73} and ψ_{80} must play an important role in the admixture because the transition contributes to $^4J_{FC}$(Se,Se) in **13**(**AA**).

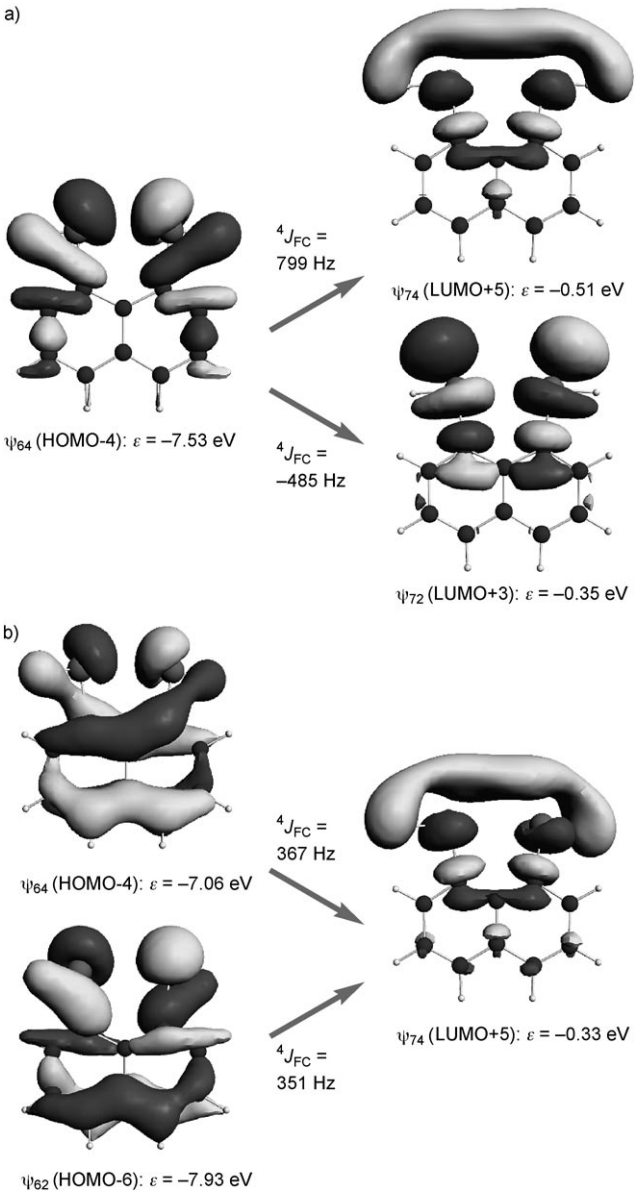

Figure 8. Selected transitions for $^4J_{FC}$(se,Se) in a) **12**(**BB**) and b) **12**(**CC**).

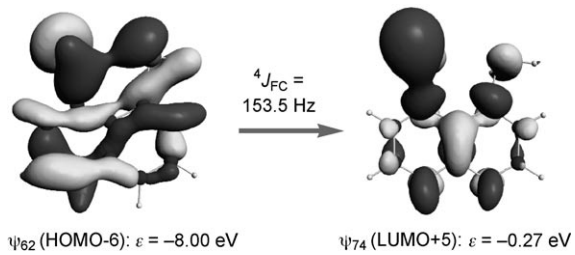

Figure 9. The $\psi_{62} \rightarrow \psi_{74}$ transition for $^4J_{FC}$(Se,Se) in **12**(**AB**).

^nJ(Se,Se) have been elucidated as through-bond ($n = 1$) and through-space mechanisms ($n = 4$). MO descriptions of the contributions from each ψ_i and $\psi_i \rightarrow \psi_a$ transition ena-

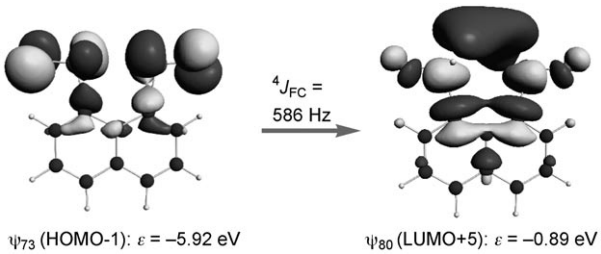

Figure 10. The $\psi_{73} \rightarrow \psi_{80}$ transition for $^4J_{FC}$(Se,Se) in **13**(**AA**).

bled us to identify and clearly visualize the origin and mechanisms of these nuclear couplings.

Analysis of ^2J(Se,Se) and ^3J(Se,Se): Figure 11 shows the optimized structures for **3a**-*gem*, **4b**-*gem*, **4b**-*cis*, **4b**-*trans*, **5a**-*gauche*, and **5a**-*anti*. ^2J(Se,Se) and ^3J(Se,Se) values were calculated by using these structures, and the results are shown in Table 5.

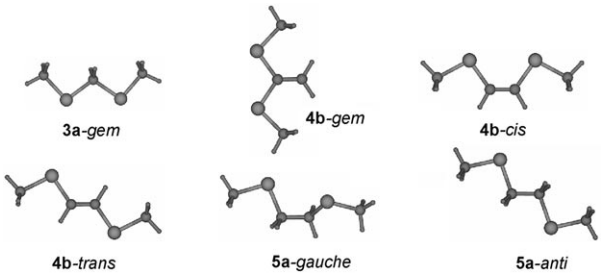

Figure 11. Optimized structures of **3a**, **4b**, and **5a**.

Table 5. Calculated values of ^2J(Se,Se) for **3a**-*gem* and **4b**-*gem* and ^3J(Se,Se) for **4b**-*cis*, **4b**-*trans*, **5a**-*gauche*, and **5a**-*anti*.[a]

	n	$^nJ_{PSO}$ [Hz]	$^nJ_{SD}$ [Hz]	$^nJ_{FC}$ [Hz]	$^nJ_{TL}$ [Hz]
3a-*gem*	2	−1.7	0.4	110.5	109.1
4b-*gem*	2	−1.8	−0.5	126.9	125.6[b]
4b-*cis*	3	−4.6	1.1	49.4	45.8[b]
4b-*trans*	3	−31.0	2.1	−33.1	−62.0[b]
5a-*gauche*	3	−1.2	6.5	36.9	42.2
5a-*anti*	3	−6.6	2.2	−34.9	−39.3

[a] $^1J_{DSO}$ was less than 0.02 Hz. [b] Values for **4a**-*gem*, **4a**-*cis*, and **4a**-*trans* (structures given in Scheme 1), see ref. [21].

Values of ^2J(Se,Se) = 109 and 126 Hz were calculated for **3a**-*gem* and **4b**-*gem*, respectively. The $^2J_{FC}$(Se,Se) term predominantly contributes to ^2J(Se,Se) in these compounds. Positive values of $^3J_{TL}$(Se,Se) = 46 and 42 Hz were predicted for **4b**-*cis* and **5a**-*gauche*, respectively. In this case, the $^3J_{FC}$(Se,Se) term predominantly contributes to $^3J_{TL}$(Se,Se). ^2J(Se,Se) in **3a**-*gem* and **4b**-*gem* and ^3J(Se,Se) in **4b**-*cis* and **5a**-*gauche* originated from n_s(Se)···n_s(Se) interactions,[32] which all have positive values. They are controlled by the FC term and the mechanisms should be closely related to those of ^4J(Se,Se). However, negative values of $^3J_{TL}$(Se,Se) = −62 and −39 Hz were predicted for **4b**-*trans* and **5a**-*anti*, respectively. The $^3J_{FC}$(Se,Se) term contributes significantly to **5a**-*anti*, whereas both the $^3J_{FC}$(Se,Se) and $^3J_{PSO}$(Se,Se) terms contribute to $^3J_{TL}$(Se,Se) in **4b**-*trans*. These results, in relation to the n_s(Se)···n_s(Se) distances, are of interest because the Se···Se distances in **4b**-*trans* and **5a**-*anti* are larger than those in **3a**-*gem*, **4b**-*gem*, **4b**-*cis*, and **5a**-*gauche*.

Torsional angular dependence was detected in ^3J(Se,Se) of **5a** that contained both conformers. Figure 12 shows the results of torsional angular dependence calculations for **5a**

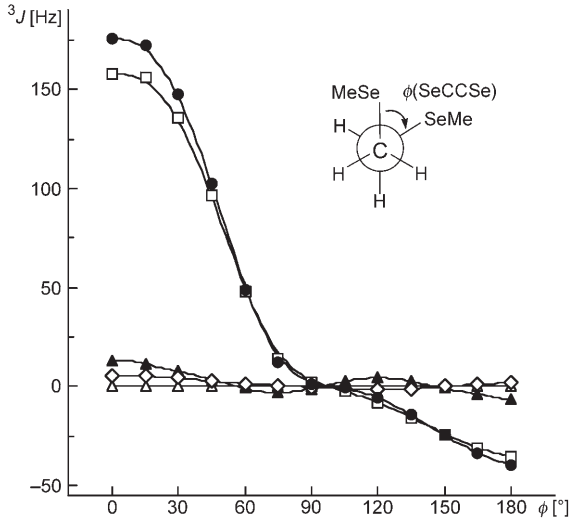

Figure 12. Torsional angular dependence of ^3J(Se,Se) in **5a**. △: $^3J_{DSO}$, ▲: $^3J_{PSO}$, ◇: $^3J_{SD}$, □: $^3J_{FC}$, and ●: $^3J_{TL}$.

that contained the structures of **5a**-*gauche* and **5a**-*anti* (Figure 11). The value of ^3J(Se,Se) in **5a** appears to depend on ϕ(SeCCSe) and its behavior must be more complex than that plotted in Figure 12 because ^3J(Se,Se) must also depend on the value of ϕ'(C_{Me}SeCC) for each half of the molecule.

It is interesting to compare the calculated and observed values of ^nJ(Se,Se) (n = 2 and 3).[21] The magnitudes of the calculated values of $^nJ_{TL}$(Se,Se) for **4b** and **4a** increase in the order *cis* < *trans* < *gem* ($^nJ_{TL}$(Se,Se) = 46, 62, and 126 Hz for **4b** and $^nJ_{TL}$(Se,Se) = 15, 42, and 89 Hz for **4a**; see Scheme 1 and Figure 11 for structures), and these values seem to be reasonable. However, there are still some discrepancies between the observed and calculated values for **4b** and **4a**, and the reasons for these discrepancies must be clarified so that ^nJ(Se,Se) can be utilitized in the study of selenium chemistry. In calculations of ^nJ(Se,Se), the structures of **4b** and **4a** must be carefully examined to explain the numerical accuracy of the values observed.[21]

Conclusion

Nuclear spin–spin coupling constants (J) provide highly important information about coupled nuclei that have strongly bonded and weakly interacting states. Values of ^nJ(Se,Se) (n = 1–4) were analyzed as the first step to investigating the nature of bonded and nonbonded interactions between Se

atoms through ^nJ(Se,Se). QC calculations were necessary for the analysis and interpretation of the J values obtained experimentally. ^nJ(Se,Se) ($n=1$–4) were analyzed by using MO theory. Structures were optimized at the DFT level by using the Gaussian 03 program and values of ^nJ(Se,Se) were calculated by employing Slater-type triple ξ basis sets at the DFT level and applying them to the optimized structures. The method employed in this work has been shown to reliably predict the values and analyze the mechanisms involved. Calculated $^nJ_{TL}$ values were composed of contributions from the $^nJ_{DSO}$, $^nJ_{PSO}$, $^nJ_{SD}$, and $^nJ_{FC}$ terms. Study of the separate terms helped us to predict the mechanisms of the spin–spin couplings, which are closely related to the electronic structures of the compounds. The main contributions from each ψ_i and $\psi_i \rightarrow \psi_a$ transition were evaluated separately.

Compound **1a** was used as a model to calculate ^1J(Se,Se), which shows a typical dependence on $\phi(C_{Me}SeSeC_{Me})$. This dependence explains the small values of $^1J_{obsd}$(Se,Se) for **1** and the large values of $^1J_{obsd}$(Se,Se) for **2**, which correspond to synperiplanar diselenides. Large $^4J_{obsd}$(Se,Se) values were also recorded for nonbonded Se···Se, Se···Se=O, and O=Se···Se=O interactions at naphthalene 1,8-positions. The main contribution to ^4J(Se,Se) is from the FC term, whereas the main contribution to ^1J(Se,Se) is from the PSO term. ^2J(Se,Se) and ^3J(Se,Se) were analyzed in a similar way, and ^3J(Se,Se) in **5a** was also found to be dependent on the torsion angle. Depending on the structure, the main contribution to ^2J(Se,Se) and ^3J(Se,Se) is from FC terms, with a smaller contribution from the PSO terms. Each transition enables us to identify and clearly visualize the origin and the mechanisms of indirect nuclear spin–spin couplings. Important molecular properties, such as electronic structures, can be clarified by elucidating the mechanisms of spin–spin coupling by using MO theory.

Similar investigations for ^nJ(P,X) are in progress and will be reported elsewhere.

Experimental Section

Chemicals were used without further purification unless otherwise stated and solvents were purified by using standard methods. Melting points were determined on a Yanako MP-S3 melting point apparatus and are uncorrected. NMR spectra were recorded at 23 °C on a JEOL AL-300 spectrometer (^{1}H, 300 MHz; ^{13}C, 75.5 MHz) and on a JEOL Lambda-400 spectrometer (^{77}Se, 76.2 MHz). The ^{1}H, ^{13}C, and ^{77}Se NMR spectra were recorded in $CDCl_3$ and [D_6]DMSO. Chemical shifts are given in ppm relative to TMS for ^{1}H and ^{13}C NMR spectra, and relative to reference compound MeSeMe for ^{77}Se NMR spectra. Column chromatography was performed by using silica gel and basic alumina.

4-Methylnaphtho[1,8-*c,d*]-1,2-diselenole (2b): Compound **2b** was prepared from 1,8-dichloro-4-methylnaphthalene by using a method similar to that previously reported for **2a**[7,11a] and was obtained as purple needles (5.10 g, 68 %). M.p. 127.0–128.0 °C; ^{1}H NMR (300 MHz, $CDCl_3$, TMS): $\delta=2.50$ (s, 3H), 7.09 (dd, $J=0.9$, 7.6 Hz, 1H), 7.25 (d, $J=7.3$ Hz, 1H), 7.36 (dd, $J=0.6$, 6.9 Hz, 1H), 7.55 ppm (dd, $J=0.7$, 8.4 Hz, 1H); ^{13}C NMR (75.5 MHz, $CDCl_3$, TMS): $\delta=18.6$, 120.4, 120.7, 121.0, 127.4, 128.2, 130.4, 137.0, 137.3, 138.0, 141.1 ppm; ^{77}Se NMR (76.2 MHz, $CDCl_3$, MeSeMe): $\delta=411.8$, 420.6 ppm; elemental analysis calcd (%) for $C_{11}H_8Se_2$: C 44.32, H 2.70; found: C 44.21, H 2.63.

4-Chloronaphtho[1,8-*c,d*]-1,2-diselenole (2c): Compound **2c** was prepared from 1,8-dichloro-4-methylnaphthalene by using a method similar to that previously reported for **2a**[7,11a] and was obtained as brown needles (3.68 g, 58 %). M.p. 155.0–156.0 °C; ^{1}H NMR (300 MHz, $CDCl_3$, TMS): $\delta=7.24$ (d, $J=8.1$ Hz, 1H), 7.30 (d, $J=7.9$ Hz, 1H), 7.34 (t, $J=7.7$ Hz, 1H), 7.39 (dd, $J=1.2$, 7.4 Hz, 1H), 7.81 ppm (dd, $J=1.3$, 7.9 Hz, 1H); ^{13}C NMR (75.5 MHz, $CDCl_3$, TMS): $\delta=120.5$, 120.6, 121.9, 127.3, 127.4, 128.6, 135.0, 138.5, 140.0, 141.2 ppm; ^{77}Se NMR (76.2 MHz, $CDCl_3$, MeSeMe): $\delta=422.6$, 444.6 ppm; elemental analysis calcd (%) for $C_{10}H_5Se_2Cl$: C 37.71, H 1.58; found: C 37.83, H 1.60.

4-Nitronaphtho[1,8-*c,d*]-1,2-diselenole (2d): Compound **2d** was prepared from 1,8-dibromo-4-nitronaphthalene by using a method similar to that previously reported for **2a**[7,11a] and was obtained as dark purple needles (2.17 g, 28 %). M.p. 196.0–197.0 °C; ^{1}H NMR (300 MHz, $CDCl_3$, TMS): $\delta=7.40$ (d, $J=8.3$ Hz, 1H), 7.52 (dd, $J=4.1$ and 7.6 Hz, 1H), 7.53 (s, 1H), 8.18 (d, $J=8.3$ Hz, 1H), 8.51 ppm (dd, $J=2.7$ and 4.1 Hz, 1H); ^{1}H NMR (300 MHz, [D_6]DMSO, TMS): $\delta=7.57$ (dd, $J=7.5$, 8.5 Hz, 1H), 7.77 (d, $J=8.5$ Hz, 1H), 7.84 (dd, $J=0.7$, 7.5 Hz, 1H), 8.20 (d, $J=8.5$ Hz, 1H), 8.29 ppm (dd, $J=0.7$, 8.5 Hz, 1H); ^{13}C NMR (75.5 MHz, [D_6]DMSO, TMS): $\delta=118.2$, 120.0, 123.4, 127.1, 129.4, 131.1, 139.0, 140.8, 144.2, 155.5 ppm; ^{77}Se NMR (76.2 MHz, $CDCl_3$, MeSeMe): $\delta=448.8$, 474.4 ppm; elemental analysis calcd (%) for $C_{10}H_5Se_2NO_2$: C 36.50, H 1.53, N 4.26; found: C 36.41, H 1.40, N 4.19.

1,8-Bis(methylselanyl)naphthalene (6): Methyl iodide (1.29 g, 9.06 mmol) was added at room temperature to a solution of the dianion of **2a**, which was prepared by reducing **2a**[7,11a] (1.03 g, 3.63 mmol) with $NaBH_4$ in aqueous THF. Water (50 mL) and dichloromethane (50 mL) were added to the solution. The organic layer was separated and washed with 5% aq. HCl, three times with water, with saturated $NaHCO_3$(aq) and again with water. After drying over Na_2SO_4, filtration, evaporation, and drying in vacuo, the crude product was purified by using column chromatography (SiO_2, hexane), then recrystallized from hexane to give **6** as colorless prisms (1.12 g, 98 %). M.p. 85.0–85.5 °C; ^{1}H NMR (300 MHz, $CDCl_3$, TMS): $\delta=2.33$ (s, 6H), 7.32 (t, $J=7.7$ Hz, 2H), 7.70 (dd, $J=1.2$, 8.2 Hz, 2H), 7.73 ppm (dd, $J=1.2$, 7.5 Hz, 2H); ^{13}C NMR (75.5 MHz, $CDCl_3$, TMS): $\delta=13.3$, 125.7, 128.3, 131.9, 132.3, 135.3, 135.6 ppm; ^{77}Se NMR (76.2 MHz, $CDCl_3$, MeSeMe): $\delta=231.4$ ppm; elemental analysis calcd (%) for $C_{12}H_{12}Se_2$: C 45.88, H 3.85; found: C 45.73, H 3.77.

1-(Methylselanyl)-8-(methylseleninyl)naphthalene (7): Compound **6** (980 mg, 3.12 mmol) was dissolved in CH_2Cl_2 (20 mL) and then bubbled with ozone for 5 min. Then the solvent was removed and the product was dried in vacuo. The crude product was purified by column chromatography (Al_2O_3, CH_2Cl_2) to give **7** as a colorless powder (875 mg, 85 %). M.p. 129.8–130.1 °C; ^{1}H NMR (300 MHz, $CDCl_3$, TMS): $\delta=2.29$ (s, 3H), 2.78 (s, 3H), 7.48 (t, $J=7.6$ Hz, 2H), 7.76 (t, $J=7.7$ Hz, 2H), 7.98–8.05 (m, 2H), 8.10 (dd, $J=1.1$, 7.2 Hz, 1H), 8.88 ppm (dd, $J=1.2$, 7.4 Hz, 1H); ^{13}C NMR (75.5 MHz, $CDCl_3$, TMS): $\delta=13.9$, 41.1, 125.7, 126.3, 126.4, 126.6, 131.0, 132.4, 133.1, 136.1, 138.9, 141.3 ppm; ^{77}Se NMR (76.2 MHz, $CDCl_3$, MeSeMe): $\delta=210.8$, 833.0 ppm; elemental analysis calcd (%) for $C_{12}H_{12}OSe_2$: C 43.66, H 3.66; found: C 43.61, H 3.60.

1,8-Bis(methylseleninyl)naphthalene (8): A solution of **6** (580 mg, 7.85 mmol) in CH_2Cl_2 (20 mL) was bubbled with ozone for 15 min. The workup was the same as that for **7**, and gave **8** as a colorless powder (377 mg, 59 %). M.p. 154.8–155.2 °C; ^{1}H NMR (300 MHz, $CDCl_3$, TMS): $\delta=2.71$ (s, 6H), 7.84 (t, $J=7.7$ Hz, 2H), 8.18 (dd, $J=1.2$, 6.9 Hz, 2H), 8.71 ppm (dd, $J=1.4$, 6.9 Hz, 2H); ^{77}Se NMR (76.2 MHz, $CDCl_3$, MeSeMe): $\delta=821.3$ ppm; elemental analysis calcd (%) for $C_{12}H_{12}O_2Se_2$: C 41.64, H 3.49; found: C 41.55, H 3.45.

1-(Methylseleninyl)-8-(phenylselanyl)naphthalene (10): Compound **10** was prepared from **9**[11a] by using a method similar to that reported above for **7** and was obtained as colorless needles (970 mg, 80 %). M.p. 129.8–130.2 °C; ^{1}H NMR (300 MHz, $CDCl_3$, TMS): $\delta=2.72$ (s, 3H), 6.98–7.02 (m, 2H), 7.11–7.16 (m, 3H), 7.56 (t, $J=7.6$ Hz, 1H), 7.76 (t, $J=7.7$ Hz, 1H), 8.05 (dd, $J=1.2$, 8.0 Hz, 1H), 8.10 (dd, $J=1.3$, 8.1 Hz, 1H), 8.15 (dd, $J=1.3$, 7.2 Hz, 1H), 8.82 ppm (dd, $J=1.3$, 7.3 Hz, 1H); ^{13}C NMR (75.5 MHz, $CDCl_3$, TMS): $\delta=40.6$, 123.2, 126.5, 126.6, 126.8, 126.9, 128.4, 129.6, 132.0, 132.4, 133.0, 133.5, 136.29, 140.9, 141.4 ppm; ^{77}Se NMR

(76.2 MHz, $CDCl_3$, MeSeMe): $\delta = 398.2$, 831.4 ppm; elemental analysis calcd (%) for $C_{17}H_{14}OSe_2$: C 52.06, H 3.60; found: C 52.11, H 3.66.

1-(Methylseleninyl)-8-(phenylseleninyl)naphthalene (11): Compound **11** was prepared from **9**[11a] by using a method similar to that reported above for **8** and was obtained as colorless needles (720 mg, 63%). M.p. 148.0–148.8 °C; ^{1}H NMR (300 MHz, $CDCl_3$, TMS): $\delta = 2.74$ (s, 3H), 7.33–7.50 (m, 3H), 7.51–7.58 (m, 2H), 7.78 (t, $J = 7.7$ Hz, 1H), 7.81 (t, $J = 7.7$ Hz, 1H), 8.13 (dd, $J = 1.1$, 8.1 Hz, 1H), 8.14 (dd, $J = 1.1$, 8.1 Hz, 1H), 8.63 (dd, $J = 1.4$, 7.4 Hz, 1H), 8.72 ppm (dd, $J = 1.3$, 7.3 Hz, 1H); ^{13}C NMR (75.5 MHz, $CDCl_3$, TMS): $\delta = 38.3$, 126.7, 126.8, 126.9, 127.0, 127.6, 127.9, 130.0, 131.7, 133.3, 133.7, 135.6, 138.9, 139.2, 141.7 ppm; ^{77}Se NMR (76.2 MHz, $CDCl_3$, MeSeMe): $\delta = 820.0$, 832.5 ppm; elemental analysis calcd (%) for $C_{17}H_{14}O_2Se_2$: C 50.02, H 3.46; found: C 50.07, H 3.57.

Acknowledgements

This work was partially supported by a Grant-in-Aid for Scientific Research (Nos. 16550038 and 19550041) from the Ministry of Education, Culture, Sports, Science, and Technology, Japan.

[1] M. Karplus, *J. Chem. Phys.* **1959**, *30*, 11–15; M. Karplus, *J. Am. Chem. Soc.* **1963**, *85*, 2870–2871.

[2] a) M. Barfield, W. B. Smith, *J. Am. Chem. Soc.* **1992**, *114*, 1574–1581; b) F. B. Mallory, C. W. Mallory, K. E. Butler, M. B. Lewis, A. Q. Xia, E. D. Luzik, Jr., L. E. Fredenburgh, M. M. Ramanjulu, Q. N. Van, M. M. Francl, D. A. Freed, C. C. Wray, C. Hann, M. Nerz-Stormes, P. J. Carroll, L. E. Chirlian, *J. Am. Chem. Soc.* **2000**, *122*, 4108–4116.

[3] T. Helgaker, M. Jaszunski, K. Ruud, *Chem. Rev.* **1999**, *99*, 293–352; H. Fukui, *Prog. Nucl. Magn. Reson. Spectrosc.* **1999**, *35*, 267-294; M. Bienati, C. Adamo, V. Barone, *Chem. Phys. Lett.* **1999**, *311*, 69–76; R. H. Contreras, J. E. Peralta, C. G. Giribet, M. C. Ruiz de Azua, J. C. Facelli in *Annual Reports on NMR Spectroscopy, Vol. 41* (Ed.: G. A. Webb), Academic Press, New York, **2000**, pp. 55–184.

[4] *Compilation of Reported ^{77}Se NMR Chemical Shifts*, (Eds.: T. M. Klapötke, M. Broschag), Wiley, New York, **1996**.

[5] Mallory and co-workers demonstrated that the value of J(F,F) becomes exponentially smaller as the nonbonded F···F distance increases. The values are controlled by spin–orbit interactions. See also ref. [2b].

[6] T. Helgaker, M. Pecul in *Calculations of NMR and EPR Parameters: Theory and Applications*, (Eds.: M. Kaupp, M. Bühl, V. G. Malkin), Wiley-VCH, Weinheim, **2004**, Chapter 7.

[7] J. Meinwald, D. Dauplaise, F. Wudl, J. J. Hauser, *J. Am. Chem. Soc.* **1977**, *99*, 255–257; J. Meinwald, D. Dauplaise, J. Clardy, *J. Am. Chem. Soc.* **1977**, *99*, 7743–7744; D. Dauplaise, J. Meinwald, J. C. Scott, H. Temkin, J. Clardy, *Ann. N. Y. Acad. Sci.* **1978**, *313*, 382–394; K. Yui, Y. Aso, T. Otsubo, *Chem. Lett.* **1986**, 551–554; Y. Aso, K. Yui, T. Miyoshi, T. Otsubo, F. Ogura, J. Tanaka, *Bull. Chem. Soc. Jpn.* **1988**, *61*, 2013–2018.

[8] A ^{77}Se NMR spectrum with a typical AB quartet pattern was observed for **2d** (Y = NO_2). After the spectrum was analyzed, a value of ^1J(Se,Se) = 330.8 Hz was obtained.

[9] Some values of $\delta(^{77}$Se) for **3**-*gem*, **5**-*gauche*, and **5**-*anti* have been reported; H. Duddeck, P. Wagner, A. Biallab, *Magn. Reson. Chem.* **1991**, *29*, 248–259, but values of ^2J(Se,Se) for **3**-*gem* and values of ^3J(Se,Se) for **5**-*gauche* and **5**-*anti* have not been reported yet.

[10] a) I. Johannsen, L. Henriksen, H. Eggert, *J. Org. Chem.* **1986**, *51*, 1657–1663; b) I. Johannsen, H. Eggert, *J. Am. Chem. Soc.* **1984**, *106*, 1240–1243.

[11] a) W. Nakanishi, S. Hayashi, S. Toyota, *Chem. Commun.* **1996**, 371–372; W. Nakanishi, S. Hayashi, S. Toyota, *J. Org. Chem.* **1998**, *63*, 8790–8800; b) S. Hayashi, W. Nakanishi, *J. Org. Chem.* **1999**, *64*, 6688–6696.

[12] See the Supporting Information.

[13] ADF 2005.01 SCM, *Theoretical Chemistry*. E. J. Baerends, J. Autschbach, A. Bérces, J. A. Berger, F. M. Bickelhaupt, C. Bo, P. L. de Boeij, P. M. Boerrigter, L. Cavallo, D. P. Chong, L. Deng, R. M. Dickson, D. E. Ellis, M. van Faassen, L. Fan, T. H. Fischer, C. Fonseca Guerra, S. J. A. van Gisbergen, J. A. Groeneveld, O. V. Gritsenko, M. Grüning, F. E. Harris, P. van den Hoek, C. R. Jacob, H. Jacobsen, L. Jensen, E. S. Kadantsev, G. van Kessel, R. Klooster, F. Kootstra, E. van Lenthe, D. A. McCormack, A. Michalak, J. Neugebauer, V. P. Nicu, V. P. Osinga, S. Patchkovskii, P. H. T. Philipsen, D. Post, C. C. Pye, W. Ravenek, P. Romaniello, P. Ros, P. R. T. Schipper, G. Schreckenbach, J. G. Snijders, M. Solà, M. Swart, D. Swerhone, G. te Velde, P. Vernooijs, L. Versluis, L. Visscher, O. Visser, F. Wang, T. A. Wesolowski, E. M. van Wezenbeek, G. Wiesenekker, S. K. Wolff, T. K. Woo, A. L. Yakovlev, and T. Ziegler, Vrije Universiteit, Amsterdam (Netherlands), **2005**.

[14] For the Slater-type orbitals, see a) E. van Lenthe, E. J. Baerends, *J. Comput. Chem.* **2003**, *24*, 1142–1156; b) D. P. Chong, E. Lenthe, S. J. A. van Gisbergen, E. J. Baerends, *J. Comput. Chem.* **2004**, *25*, 1030-1036.

[15] Gaussian 03, Revision D.02, M. J. Frisch, G. W. Trucks, H. B. Schlegel, G. E. Scuseria, M. A. Robb, J. R. Cheeseman, J. A. Montgomery, Jr., T. Vreven, K. N. Kudin, J. C. Burant, J. M. Millam, S. S. Iyengar, J. Tomasi, V. Barone, B. Mennucci, M. Cossi, G. Scalmani, N. Rega, G. A. Petersson, H. Nakatsuji, M. Hada, M. Ehara, K. Toyota, R. Fukuda, J. Hasegawa, M. Ishida, T. Nakajima, Y. Honda, O. Kitao, H. Nakai, M. Klene, X. Li, J. E. Knox, H. P. Hratchian, J. B. Cross, V. Bakken, C. Adamo, J. Jaramillo, R. Gomperts, R. E. Stratmann, O. Yazyev, A. J. Austin, R. Cammi, C. Pomelli, J. W. Ochterski, P. Y. Ayala, K. Morokuma, G. A. Voth, P. Salvador, J. J. Dannenberg, V. G. Zakrzewski, S. Dapprich, A. D. Daniels, M. C. Strain, O. Farkas, D. K. Malick, A. D. Rabuck, K. Raghavachari, J. B. Foresman, J. V. Ortiz, Q. Cui, A. G. Baboul, S. Clifford, J. Cioslowski, B. B. Stefanov, G. Liu, A. Liashenko, P. Piskorz, I. Komaromi, R. L. Martin, D. J. Fox, T. Keith, M. A. Al-Laham, C. Y. Peng, A. Nanayakkara, M. Challacombe, P. M. W. Gill, B. Johnson, W. Chen, M. W. Wong, C. Gonzalez, J. A. Pople, Gaussian, Inc., Wallingford CT, **2004**.

[16] a) J. A. Anderson, J. D. Odom, A. J. Zozulin, *Organometallics* **1984**, *3*, 1458–1465; b) G. Llabres, M. Baiwir, J.-L. Piette, L. Christiaens, *Org. Magn. Reson.* **1981**, *15*, 152–154.

[17] For the 6-311G(3df) basis sets, see: a) R. C. Binning, Jr., L. A. Curtiss, *J. Comput. Chem.* **1990**, *11*, 1206–1216; b) L. A. Curtiss, M. P. McGrath, J.-P. Blaudeau, N. E. Davis, R. C. Binning, Jr., L. Radom, *J. Chem. Phys.* **1995**, *103*, 6104–6113; c) M. P. McGrath, L. Radom, *J. Chem. Phys.* **1991**, *94*, 511–516; for the diffuse functions (+ and ++), see T. Clark, J. Chandrasekhar, G. W. Spitznagel, P. v. R. Schleyer, *J. Comput. Chem.* **1983**, *4*, 294–301.

[18] a) A. D. Becke, *Phys. Rev. A* **1988**, *38*, 3098–3100; A. D. Becke, *J. Chem. Phys.* **1993**, *98*, 5648–5652; b) C. Lee, W. Yang, R. G. Parr, *Phys. Rev. B* **1988**, *37*, 785–789; B. Miehlich, A. Savin, H. Stoll, H. Preuss, *Chem. Phys. Lett.* **1989**, *157*, 200–206.

[19] The DFT level here was employed to optimize the structures because it was supplied by the ADF program that we used. However, the DFT level should be carefully employed for systems that contain nonbonded interactions. DFT could not evaluate the nonbonded interactions correctly because most functionals are not treated by the exchange-correlation functional. For examples, see a) C. Bleiholder, D. B. Werz, H. Köppel, R. Gleiter, *J. Am. Chem. Soc.* **2006**, *128*, 2666–2674; b) C. Bleiholder, R. Gleiter, D. B. Werz, H. Köppel, *Inorg. Chem.* **2007**, *46*, 2249–2260.

[20] Values of J were also satisfactorily calculated by using the Gaussian 03 program in most cases.

[21] The structures of **4a**-*gem*, **4a**-*cis*, and **4a**-*trans* (Scheme 1) were also optimized by employing the 6-311++G(3df,2pd) basis sets of the Gaussian 03 program at the DFT (B3LYP) level. The values of $^2J_{TL}$(Se,Se) and $^3J_{TL}$(Se,Se) were also calculated for structures of **4a**-*gem*, **4a**-*cis*, and **4a**-*trans* with appropriate substituents. The values were 88.5, 15.1, and −41.8 Hz for **4a**-*gem*, **4a**-*cis*, and **4a**-*trans*, re-

spectively, although these optimized structures might not be the global minima. Details of this will be discussed elsewhere.

[22] a) E. van Lenthe, E. J. Baerends, J. G. Snijders, *J. Chem. Phys.* **1993**, *99*, 4597–4610; b) E. van Lenthe, E. J. Baerends, J. G. Snijders, *J. Chem. Phys.* **1994**, *101*, 9783–9792; c) E. van Lenthe, A. Ehlers, E. J. Baerends, *J. Chem. Phys.* **1999**, *110*, 8943–8953.

[23] The value of ^{1}J(Se,Se) that was calculated for **2a** at the nonrelativistic level was smaller than that obtained with the scalar ZORA relativistic formulation, whereas the value of ^{4}J(Se,Se) for **12**(**AA**) that was calculated at the nonrelativistic level was several magnitudes larger than that obtained with the scalar ZORA relativistic formulation. The values calculated at the nonrelativistic level seem to be closer to the observed values than those obtained with the scalar ZORA relativistic formulation in our calculation system. Therefore, it would be reasonable in this case to discuss the values of ^{n}J(Se,Se) calculated at the nonrelativistic level.

[24] a) J. Autschbach, T. Ziegler, *J. Chem. Phys.* **2000**, *113*, 936–947; b) J. Autschbach, T. Ziegler, *J. Chem. Phys.* **2000**, *113*, 9410–9418.

[25] A plot of the contributions from ψ_{39}–ψ_{43} (y axis) versus those from ψ_{1}–ψ_{43} (x axis) shows an excellent correlation ($y=0.976x+37.3$: $r^2=0.9999$).

[26] Some vacant MOs (ψ_a), such as those at ψ_{395}, ψ_{396}, ψ_{435}, and ψ_{436}, also contribute to $^{4}J_{PSO}$(Se,Se) in **2a**. However, the contributions from these vacant MOs are cancelled out by the addition of contributions from other nearby orbitals. For example, the magnitude of the contributions from ψ_{301}–ψ_{438} to $^{4}J_{PSO}$(Se,Se) amounts to less than 0.3 Hz, of which ψ_{438} has the highest energy.

[27] 1,8-Bis(selanyl)naphthalenes have some conformers, mainly **CC** and **AB**.[33] Nonbonded interactions will contribute significantly to ^{4}J(Se,Se) because n_s(Se) plays an important role in ^{4}J(Se,Se).

[28] Although 1,8-bis(methylselanyl)naphthalene and 1-(methylselanyl)-8-(phenylselanyl)naphthalene were observed as the **CC** conformer in the solid state, **AB** conformers must also be present and contribute in solution, which has an effect on ^{4}J(Se,Se).

[29] W. Nakanishi, S. Hayashi, unpublished results.

[30] The motion of the lowest frequency in the **BB** conformer leads to the **CC** conformer. The second lowest frequency corresponds to the rotation around the C_{2v} axis in the **BB** conformer, which maintains the plane of the C_{Me}, Se, Se, and C_{Me} atoms with the naphthyl plane moving in the opposite direction.

[31] Although not shown, ψ_{72} (HOMO) and the $\psi_{72}\rightarrow\psi_{82}$ transition mainly contribute to $^{4}J_{FC}$(Se,Se) in **6**(**CC**) and **6**(**AB**). Similarly, the contributions from ψ_{84} (HOMO) and the $\psi_{84}\rightarrow\psi_{92}$ transition explain the values of $^{4}J_{FC}$(Se,Se) in **8**(**AA**).

[32] The importance of the direction of the s-type lone-pair orbital of Se in ^{2}J(Se,C) is well established; see: a) W. Nakanishi, Y. Ikeda, *Bull. Chem. Soc. Jpn.* **1983**, *56*, 1661–1664; b) H. J. Reich, J. E. Trend, *J. Chem. Soc. Chem. Commun.* **1976**, 310–311.

[33] W. Nakanishi, S. Hayashi, T. Uehara, *J. Phys. Chem. A* **1999**, *103*, 9906–9912.

Received: September 28, 2007
Revised: February 25, 2008
Published online: April 30, 2008

